Consistency of Estimated Global Water Cycle Variations over the Satellite Era

F. R. ROBERTSON,* M. G. BOSILOVICH,+ J. B. ROBERTS,* R. H. REICHLE,+ R. ADLER,#
L. RICCIARDULLI,@ W. BERG,& AND G. J. HUFFMAN**

* *Earth Science Office, NASA Marshall Space Flight Center, Huntsville, Alabama*
+ *Global Modeling and Assimilation Office, NASA Goddard Space Flight Center, Greenbelt, Maryland*
# *Earth System Science Interdisciplinary Center, University of Maryland, College Park, College Park, Maryland*
@ *Remote Sensing Systems, Santa Rosa, California*
& *Department of Atmospheric Science, Colorado State University, Fort Collins, Colorado*
** *Mesoscale Atmospheric Processes Laboratory, NASA Goddard Space Flight Center, Greenbelt, Maryland*

(Manuscript received 2 July 2013, in final form 14 April 2014)

ABSTRACT

Motivated by the question of whether recent interannual to decadal climate variability and a possible ''climate shift'' may have affected the global water balance, we examine precipitation minus evaporation ($P - E$) variability integrated over the global oceans and global land for the period 1979–2010 from three points of view—remotely sensed retrievals and syntheses over the oceans, reanalysis vertically integrated moisture flux convergence (VMFC) over land, and land surface models (LSMs) forced with observations-based precipitation, radiation, and near-surface meteorology.

Over land, reanalysis VMFC and P − evapotranspiration (ET) from observationally forced LSMs agree on interannual variations (e.g., El Niño/La Niña events); however, reanalyses exhibit upward VMFC trends 3–4 times larger than P − ET trends of the LSMs. Experiments with other reanalyses using reduced observations show that upward VMFC trends in the full reanalyses are due largely to observing system changes interacting with assimilation model physics. The much smaller P − ET trend in the LSMs appears due to changes in frequency and amplitude of warm events after the 1997/98 El Niño, a result consistent with coolness in the eastern tropical Pacific sea surface temperature (SST) after that date.

When integrated over the global oceans, E and especially P variations show consistent signals of El Niño/La Niña events. However, at scales longer than interannual there is considerable uncertainty especially in E. This results from differences among datasets in near-surface atmospheric specific humidity and wind speed used in bulk aerodynamic retrievals. The P variations, all relying substantially on passive microwave retrievals over ocean, also have uncertainties in decadal variability, but to a smaller degree.

1. Introduction

Quantifying the global hydrological cycle and its variability across various time scales remains a challenge to the climate community. Direct measurements of evaporation (E), evapotranspiration (ET), and precipitation (P) are not feasible on a global scale, nor is the transport of water vapor over the global oceans and sparsely populated land areas. These constraints have necessitated heavy reliance on data assimilation and remote sensing, actually spurring great advances in both of these enterprises. From early efforts relying on conventional surface and aerological observations (e.g., Baumgartner and Reichel 1975; Rosen and Omolayo, 1981; Peixoto and Oort 1992) to more recent studies using reanalysis products (Trenberth et al. 2007, 2011; see also references therein), and satellite remote sensing (Schlosser and Houser 2007; Wentz et al. 2007; Wong et al. 2011), improved estimates of various fluxes and their climatological means and variability have been achieved.

Expanding satellite data streams have enabled development of water (and energy) flux products, complementing reanalyses and facilitating observationally constrained modeling. For example, precipitation from the Global Precipitation Climatology Project (GPCP; Adler et al. 2003; Huffman et al. 2009), the National Oceanic and Atmospheric Administration (NOAA) Climate Prediction Center unified precipitation analysis (CPCU; M. Chen et al. 2008), and refinement of the

Corresponding author address: F. R. Robertson, Earth Science Office, NASA Marshall Space Flight Center, 320 Sparkman Dr., Huntsville, AL 35805.
E-mail: pete.robertson@nasa.gov

DOI: 10.1175/JCLI-D-13-00384.1

complementary Global Precipitation Climatology Centre (GPCC) gauge-based analysis (Becker et al. 2013) are used to force terrestrial hydrologic cycle models (e.g., Rodell et al. 2004; Dirmeyer et al. 2006; Qian et al. 2006; Reichle et al. 2011) that synthesize global estimates of runoff, moisture storage, and evapotranspiration on scales of 100 km or less. Latent heat flux retrievals (Shie et al. 2012; Clayson et al. 2014, manuscript submitted to *Int. J. Climatol.*) and their blending with reanalysis estimates (Yu et al. 2008) are now routinely provided over the global oceans.

But evolution of the global observing system has produced complications. Satellite observations became available only in the late 1970s and subsequent improvements in resolution and accuracy have resulted in "epochs" of observational quasi-uniformity that can adversely affect reanalyses. Biases from model physical parameterizations affecting reanalysis water and energy fluxes only get corrected if accurate observations are available. Robertson et al. (2011), Lorenz and Kunstmann (2012), and Trenberth et al. (2011) each detail the problem of discrete changes in satellite observing systems and the resulting introduction of artificial steps or trends in P and E time series both over ocean and land. To varying degrees this nonstationarity in the observing system also plagues remotely sensed flux products.

A number of recent papers have evaluated progress in closing the global water cycle. Schlosser and Houser (2007) used satellite-based observations to assess global water cycle closure from a satellite perspective, concluding that improvements in accuracy of twofold to an order of magnitude were needed to close the global water budget. Sheffield et al. (2009) detailed the effects of precipitation biases in a study of hydrologic balance over the Mississippi basin. Through collaborations within the National Aeronautics and Space Administration (NASA) Energy and Water Cycle Study (NEWS) Program climatological uncertainties in satellite remotely sensed water and energy flux uncertainties are being further quantified and reduced, both regionally and globally (e.g., T. L'Ecuyer et al. 2014, unpublished manuscript; M. Rodell et al. 2014, unpublished manuscript).

While efforts to "close" the global hydrologic cycle (i.e., to eliminate budget residuals) continue to reduce uncertainties, emphasis on the modes of water cycle *variability* and links to climate has arguably become the problem of leading importance. The major thrust of this paper is to ask: Over the 30-plus years of the satellite record to what extent are there consistent interannual to decadal variations in E/ET and P and implied ocean–land moisture transport averaged over global land and ocean? ENSO-related changes in precipitation distribution between ocean and land have long been recognized (e.g., Ropelewski and Halpert 1987; Dai et al. 1997; Gu et al. 2007). While these events frequently have sharp year-to-year changes, the time scale of ENSO ranges from approximately 2 to 7 years with fluctuations in amplitude and frequency on multidecadal time scales. Trenberth and Hurrell (1994), Zhang et al. (1997), and Deser et al. (2004) have highlighted lower frequency ENSO-like variability in Pacific sea surface temperatures (SSTs) and surface pressure, i.e., Pacific decadal variability (PDV). Barlow et al. (2001) and Dai (2013) have tied drought in the southwestern United States to PDV signals in SST. The occurrence of a climate shift in the late 1990s toward a "La Niña–like" SST pattern has been explored by Burgman et al. (2008) and J. Chen et al. (2008), illustrating PDV expressions in the variability of water vapor, precipitation and cloud radiative flux over the Pacific basin. More recently Gu and Adler (2013) addressed coupled changes in SST, column-integrated water vapor and precipitation during the post-1988 era and related these changes to the change in PDV phase near or just after the large 1997/98 ENSO warm event. The role of this recent "climate shift" in producing East African rainfall declines and dislocations around the Indian Ocean rim nations has also been noted by Lyon and DeWitt (2012) and Lyon et al. (2013). Given the admittedly short ~30-yr record for most of our datasets, and the presence of embedded sensor change artifacts, to what extent are variations in P and E accompanying this PDV phase change reflected in global land and ocean area means?

The paper is organized as follows: In section 2 we detail the methodology and the datasets used, including some commentary on observing system changes that affect our results. Section 3 considers E and P retrieved over the global oceans, delving into aspects of algorithm uncertainties and the origin of disparities between different datasets. Section 4 considers reanalyses and observationally forced offline land surface models and addresses the nature of reanalysis trends in ocean–land moisture transport. Section 5 puts the entirety of these results into perspective vis-à-vis implications for detecting interannual signals and the recent PDV phase shift. Final comments are offered in section 6 along with some suggested research priorities.

2. Methodology and datasets

a. Analysis approach

Our analysis strategy is to integrate three largely independent types of data: (i) satellite retrievals and syntheses of freshwater flux $E - P$ over the global ocean, (ii) vertically integrated moisture convergence (VMFC) over land from state-of-the-art reanalyses and related

model experiments, and (iii) $P - ET$ also over land, estimated from a diagnostic ET dataset based on either satellite-driven flux retrievals or offline terrestrial hydrologic models forced with reanalysis data that has been heavily constrained by observations-based precipitation, radiation, and near-surface meteorology. We refer to these two approaches, collectively, as land surface models (LSMs). Since our analysis uses monthly-mean data, near-global atmospheric moisture storage changes are very small on these scales; and since the global integral of moisture transport must approach zero, $E - P$ over ocean should equal $P - ET$ over land (after adjusting for ocean and land areas). The land surface and diagnostic models of ET do not include Antarctica or much of Greenland. Accordingly, we limit our calculations to the 60°N/S domain. Using reanalysis datasets we have verified that this assumption does not significantly affect our results. This is due in part to water vapor typically being much smaller at higher latitudes. We will focus on these area-integrated quantities, realizing of course, that resolution of differences and inconsistencies noted here will require more detailed analysis in space, time and weather regime[1] and a continued scrutiny of algorithms.

b. Datasets

In this section we highlight details of the datasets used in this study. Because the nature of our analysis depends on a substantial number of datasets we provide in Table 1 a brief listing of their key attributes and references. Prior to our calculations all data were regridded to a 1.0° latitude–longitude grid.

1) P AND E OVER OCEAN

Precipitation estimates over the ocean rely heavily on passive microwave measurements from the Special Sensor Microwave Imager (SSM/I) constellation providing coverage since late 1987. This includes the follow-on Special Sensor Microwave Imager/Sounder (SSM/IS) series. We will appeal to three algorithms: the GPCP version 2.2 (V2.2) product (Adler et al. 2003; 2012; Huffman et al. 2009), the Goddard profiling algorithm (GPROF; Kummerow et al. 2001, 2011), and the version 7 update of the Remote Sensing Systems (RSS) precipitation product (Hilburn and Wentz 2008; Wentz 2013), referred to herein as RSS V7.

Each of these algorithms depends primarily on emission by liquid water inducing a warming signal over the radiometrically cold ocean background. There are a number of differences, however, that build in some level of independence between the products. GPCP uses an emission-based algorithm (Wilheit et al. 1991) that fits a lognormal distribution to the daily sampled rain rates and uses only the 0600 and 1800 local equatorial crossing time for SSM/I and/or SSM/IS sensors (*F8*, *F11*, *F13*, and *F17*) to minimize diurnal sampling effects. This microwave-only product is then used to calibrate an infrared (IR) precipitation index from geostationary and polar orbiting sensors, which reduces sampling error. At higher latitudes over ocean an empirical technique using low-orbit satellite microwave/IR sounder information is blended in where the SSM/I- and SSM/IS-based algorithms are judged as significantly underestimating precipitation magnitude. Before the July 1987 start of SSM/I passive microwave data an alternative scheme is used—the outgoing longwave radiation (OLR) precipitation index (OPI; Janowiak and Xie 1999), which correlates OLR anomalies with precipitation anomalies, is climatologically calibrated to the GPCP data during the SSM/I era (1988–2007). Over land the satellite estimates are strongly constrained by the gauge analysis from the GPCC (Schneider et al. 2014; Becker et al. 2013).

GPROF 2010 is a generic algorithm designation for the current update to the operational Tropical Rainfall Measuring Mission (TRMM) passive microwave retrieval algorithm that employs a Bayesian estimation method in conjunction with an a priori library of TRMM radar (2a25 V7 algorithm) and cloud resolving model rain rate–brightness temperature relationships to arrive at a most likely rainfall rate (Kummerow et al. 2011). GPROF 2010 V1a is the update used in this study for the SSM/I implementation of this algorithm, which uses all seven channels to relate the brightness temperature vector to the most likely rain rate. As such, it recognizes both the emission signals as well as scattering of upwelling radiation by frozen hydrometeors in the upper troposphere and at higher latitudes. Over oceans, this version of the GPROF algorithm uses 2a25 V7 estimates in the a priori database, and thus most of the development and analysis of GPROF algorithm versions has focused on tropical/subtropical regions within the 37.5°N/S coverage of the TRMM spacecraft. Outside of this region the algorithm relies on an extended database, which modifies the radar-observed profiles for the colder scenes not observed within the TRMM region.

RSS V7 (Wentz 2013) is the most recent update of an earlier retrieval system (Hilburn and Wentz 2008). The retrievals account for emission and scattering properties of liquid and frozen hydrometeors, column-integrated water vapor and surface wind speed. RSS V7 embodies major changes to the radiative transfer model, refined

[1] By weather regime we mean stratification or clustering of states based on cloud properties, moisture, vertical motion, or other distinguishing attributes.

TABLE 1. Datasets used in the investigation and key properties. See section 2 for discussion and references for additional details.

	Dataset	Native resolution	Physical basis/attributes	References	Comments
Remotely sensed precipitation	GPCP	2.5° global (1979–present)	Passive micowave emission calibrates IR	Adler et al. (2003, 2012)	Tied to GPCC over land
	RSS V7	0.25° ocean only (Jul 1987–present)	Unified passive micowave	Hilburn and Wentz (2008); Wentz (2013)	Tbs intercalibrated but sampling uncertainties remain
	GPROF 2010 V1a	0.25° global (Jul 1987–2009)	Bayesian passive microwave	Kummerow et al. (2001, 2011)	Lookup table uses TRMM PR
Remotely sensed ocean evaporation	OAFlux	1.0° (1959–present)	OI blend of reanalysis and satellite with buoy constraints	Yu et al. (2008), COARE 3.0 retrieval, Reynolds et al. (2007), SST and reanalyses	RSS V6 SSM/I; V7 SSM/IS, WindSat, AMSR-E; V4 QuikSCAT
	GSSTF3	1.0° (Jul 1987–2009)	Passive microwave drives COARE 3.0 bulk aero model	Shie et al. (2009, 2012)	NCEP–DOE Reanalysis 2 Reynolds SST
	SeaFlux	0.25° (1998–2007)	Neural net retrievals drive COARE 3.0 bulk aero model	Roberts et al. (2010); Clayson et al. (2014, manuscript submitted to *Int. J. Climatol.*)	Reynolds and Smith SST with diurnal cycle
Observation-driven land surface models	GLDAS-2 Noah	0.5° (1948–present)	Driven by Sheffield et al. (2006) "Princeton forcing"	Rodell et al. (2004)	Surface obs correct NCEP–NCAR forcing
	GLDAS VIC	1.0° (1948–2006)	Driven by earlier version of Princeton forcing	Sheffield et al. (2006); Sheffield and Wood (2007)	Surface obs correct NCEP–NCAR forcing
	MPI-BGC	0.5° (1982–2011)	Scaling-up of FLUXNET via machine learning algorithm	Jung et al. (2009, 2010)	GPCC precipitation used for classification
	GPCC	0.5°	67 200 gauges world wide	Schneider et al. (2014)	Gauge only
	MERRA-Land	0.625° lon, 0.5° lat (1979–present)	Offline version of MERRA catchment LSM	Reichle et al. (2011, 2014)	CPCU precipitation
Reanalysis and reduced observation (REDOBS) experiments	MERRA	0.625° lon, 0.5° lat (1979–present)	GEOS-5; Incremental Analysis Update (IAU)	Rienecker et al. (2011)	Balanced budgets recoverable
	ERA-I	1.0° (1979–2010)	ECMWF Integrated Forecast System (IFS Cy31r2)	Dee et al. (2011)	VMFC as corrected by NCAR CAS (Trenberth et al. 2011)
	CFSR	1.0° (1979–2010)	Weak ocean–atmosphere coupling	Saha et al. (2010)	
	GEOS-5 F25c72	2.5° lon, 2.0° lat (1979–2012)	Specified observed SST	Molod et al. (2012)	http://gmao.gsfc.nasa.gov/
	ECMWF 20CM	1.875° (1900–2009)	Specified observed SST	http://www.ecmwf.int/research/era/do/get/index	http://apps.ecmwf.int/datasets/data/era20cm_moda/
	NOAA 20CR	2.0° (1871–present)	Specified observed SST and surface pressure assimilated	Compo et al. (2011)	http://www.esrl.noaa.gov/psd/data/20thC_Rean/
Ocean surface wind speed	RSS V7	0.25° (Jul 1987–present)	Emission warming from wind-induced capillary waves	Hilburn and Wentz (2008); Wentz (2013)	Improved intercalibration reduces wind speed trend
	CCMP	0.25° (Jul 1987–present)	Variationally blends RSS V6 passive and active microwave sensors retrievals	Atlas et al. (2011)	SeaFlux uses L-2 swath winds before variational blending

sensor calibration, and a better treatment of footprints partially filled with hydrometeors. These improvements resulted in a greater than fifteen percent increase in precipitation over the previous V6 product, almost exclusively over the middle and high latitudes.

Microwave frequencies on the SSM/I series also enable wind speed and near-surface humidity retrievals, information critical to constructing the ocean evaporation/latent heat flux datasets we will use: the Goddard Satellite-Based Surface Turbulent Flux product, version 3 (GSSTF3; Shie et al. 2009, 2012); the Objectively Analyzed Air–Sea Fluxes (OAFlux; Yu and Weller 2007; Yu et al. 2008); and the newly released SeaFlux algorithm (Roberts et al. 2010; Clayson et al. 2014, manuscript submitted to *Int. J. Climatol.*). More specifics on inputs to these datasets are provided in Table 1. The physical models for exchange at the surface in each of these datasets (e.g., COARE 3.0 bulk turbulent flux algorithm, Fairall et al. 2003) are maturing, but input drivers of near-surface meteorology are still uncertain. In the bulk formula approach E is modeled as

$$E = C_E \rho_a U[q_s(\mathrm{SST}) - q_a], \tag{1}$$

where C_E is the exchange coefficient, ρ_a is air density, U is 10-m wind speed, and $q_s(\mathrm{SST}) - q_a$ is the moisture deficit (Δq) between the saturation specific humidity at the ocean surface and the specific humidity of the near-surface air. Near-surface humidity can only be retrieved indirectly from these sensors because SSM/I frequencies function as window channels and cannot directly capture vertical structure within and across the planetary boundary layer. GSSTF3 (Shie et al. 2009, 2012) is the latest version of the original SSM/I-based algorithm developed by Chou et al. (1995, 2001, 2003) and now employs the Bentamy et al. (2003) algorithm for near-surface q_a retrieval. In making geophysical retrievals, information on Earth incidence angle (EIA) variations (Hilburn and Shie 2011) accompanying the T_b values must be used. EIA data account for spacecraft altitude decay and precession of the orbit perigee (lowest altitude). These data have been used in retrieving GSSTF3 q_a yielding reduced q_a biases compared to those in GSSTF2b (Shie et al. 2012). Version 6 (V6) RSS 10-m wind speeds (which embody EIA corrections) are used along with sea surface temperature (SST) taken from the National Centers for Environmental Prediction (NCEP)–U.S. Department of Energy (DOE) Reanalysis 2 (Kanamitsu et al. 2002).

Alternatively, global reanalyses offer dynamical constraints of assimilated near-surface meteorology and other observations, but are also subject to uncertainties and biases in model parameterized physics of boundary layer turbulent transport, convection, and other related processes. These biases remain less constrained over the oceans where direct near-surface observations are sparse. OAFlux (Yu and Weller 2007; Yu et al. 2008) blends reanalysis and direct satellite retrieval of winds and near-surface meteorology (10-m wind, 2-m q_a and air temperature, and SST) from each source within an optimal interpolation adjustment strategy; these quantities subsequently drive the Coupled Ocean–Atmosphere Response Experiment (COARE) 3.0 algorithm. NOAA optimum interpolation (OI) 0.25° daily SST is used to derive q_s. The National Oceanography Centre (NOC) climatological atlas of International Comprehensive Ocean–Atmosphere Data Set (ICOADS) data (Josey et al. 1998) and a large number of buoys are used to estimate error covariances and weights for the variational analysis and to enforce bias reduction. Time mean OAFlux buoy bias is of order $1.0\,\mathrm{W\,m^{-2}}$ and the mean absolute difference is $7.4\,\mathrm{W\,m^{-2}}$ (Yu et al. 2008).

We also consider the much shorter (1998–2007) record of the SeaFlux product (Roberts et al. 2010; Clayson et al. 2014, manuscript submitted to *Int. J. Climatol.*) because the error estimates of this state-of-the-art algorithm compared to in situ buoys are the lowest of current satellite algorithm estimates. This product relies on intercalibrated SSM/I observations produced at Colorado State University (http://rain.atmos.colostate.edu/FCDR), but EIA corrections have not been incorporated. SeaFlux uses a neural network-based method to retrieve near-surface meteorology and has a diurnally varying component of SST (Clayson and Bogdanoff 2013). Wind speeds are derived from the cross-calibrated multiplatform (CCMP) wind swath level product (Atlas et al. 2011) to which 6-hourly analyzed wind directions have been assigned but wind magnitude remains unadjusted. Thus, wind speeds from SeaFlux are best characterized as a multisensor average of wind speed retrievals from SSM/I V6, TRMM Microwave Imager (TMI) version 4 (V4), and Advanced Microwave Scanning Radiometer for Earth Observing System (AMSR-E) version 5 (V5) available from RSS. SeaFlux also employs MERRA tendencies in near-surface q_a to interpolate changes between satellite sampling times.

Other ancillary datasets are used to aid in our dataset assessments. Monthly-mean 10-m ocean wind speeds from the CCMP wind product (Atlas et al. 2011) are produced by blending RSS V6 SSM/I, AMSR-E, TMI, and Quick Scatterometer (QuikSCAT) V4 wind speed retrievals together with a reanalysis first-guess. A merged set of all microwave-based wind speed retrievals for climate analysis is also under development at RSS. As an interim product we applied their tentative scaling adjustments as shown in Table 2 to *F8*, *F11*, *F13*, and *F17*. These sensors were chosen so as to maintain

TABLE 2. Multiplicative scaling coefficients (A) and offsets (B) used to intercalibrate RSS wind speeds from various SSM/I and SSM/IS sensors relative to *F13*. Values are tentative determinations and may change in the final RSS product.

Scaling parameter	*F8*	*F10*	*F11*	*F13*	*F17*
A	0.017	0.084	0.064	0.00	−0.024
B	1.002	0.990	0.993	1.00	0.998

sampling as close as possible to the nominal 0600 and 1800 local equatorial crossing times and minimize diurnal cycle aliasing. As in the case of precipitation retrievals, it is important to note that this is only twice-a-day sampling in most locations, not globally complete sampling on any given day.

2) REANALYSES

Vertically integrated moisture flux convergence, VMFC, comes from three state-of-the-art reanalysis projects—the NASA Modern-Era Retrospective Analysis for Research and Applications (MERRA; Rienecker et al. 2011); the European Centre for Medium Range Weather Forecasting (ECMWF) Interim Re-Analysis (ERA-Interim, herein ERA-I; Dee et al. 2011) and the NCEP Climate Forecast System Reanalysis (CFSR; Saha et al. 2010). For ERA-I and CFSR, we use the monthly-mean VMFC gridded fields computed from pressure level analyses by Trenberth et al. (2011) and obtained from the National Center for Atmospheric Research (NCAR) Climate Analysis Section (CAS) data holdings. MERRA VMFC was computed from the model level data during the integration and archived as a reanalysis product.

A consistent finding of reanalysis studies is that VMFC is a more reliable quantity than the model physics-derived $E - P$ (Trenberth and Guillemot 1998; Trenberth et al. 2011). This is due principally to the fact that water vapor and wind are state variables in the analysis system and are driven largely by rawinsonde profile measurements of these quantities, especially over land. Time-dependent biases in model E and P arise from imperfect model representations of complex physical processes interacting with changes in the observing system that are heavily weighted toward satellite moisture and temperature (Robertson et al. 2011). In general, atmospheric moisture budgets do not balance unless the moisture analysis increment is taken into account. Significant uncertainties in VMFC can remain over land even with the greater density of constraining rawinsonde data there. Observations are far from homogeneous, with highest rawinsonde densities over North America and Europe but particularly large gaps over southern hemispheric and tropical continental regions. The frequency of wind measurements ingested from aircraft and wind profiler systems also increases significantly with time. Globally, VMFC must vanish (by Green's theorem) so VMFC integrated over land (accounting for fractional coverage of land versus water) is the negative of that quantity over ocean.

Monthly VMFC data during the 1979–2012 period from several model integrations using only reduced observational constraints (REDOBS experiments) are also analyzed: the ECMWF twentieth-century reanalysis (20CM), an integration of the NASA Goddard Earth Observing System Model (GEOS-5) Fortuna version F25c72 (Molod et al. 2012), and the NOAA twentieth-century reanalysis (20CR; Compo et al. 2011). The former two integrations employ observed SST and observed sea ice only while the latter also assimilates surface pressure. Comparing the implied moisture transport (land $P - \mathrm{ET}$) in these experiments to that of the full reanalyses provides one measure of how data assimilation uncertainties affect longer terms trends. At the same time estimates of the influence of SST forcing alone on moisture transport can be studied.

3) OBSERVATIONALLY CONSTRAINED LAND SURFACE MODELS

Observationally constrained land modeling can provide a third perspective on moisture transport. Here we consider ET from several of these sources. One approach is based on simulations using prognostic LSMs typically run as components of coupled global models, but configured to run in "offline" mode and forced with observed precipitation and typically with radiation and near-surface meteorology that has been corrected with in situ and/or satellite. Version 2 of the Global Land Data Assimilation System initiative (GLDAS-2; Rodell et al. 2004), provides assimilated land surface states, energy, and water fluxes for an array of LSMs using a uniform forcing dataset (Sheffield et al. 2006; hereafter called "Princeton forcing"). At the time of this study only the Noah model component of GLDAS-2 was available for the period 1979–present. We have also used the 1979–2000 portion of an earlier GLDAS effort (Sheffield and Wood 2007) using the variable infiltration capacity (VIC) model (Liang et al. 1996, 2003) and a shorter, earlier version of the Princeton forcing data. This forcing dataset is constructed by combining a suite of global observation-based datasets with the NCEP–NCAR reanalysis. Known biases are corrected using observation-based precipitation, air temperature and radiation from the GPCP, TRMM, University of East Anglia Climatic Research Unit, and NASA Langley surface radiation budget datasets.

A closely related effort, MERRA-Land (Reichle et al. 2011, 2014), is in fact an "offline" replay of the MERRA land model component with two key changes from the

original MERRA reanalysis: 1) Its precipitation forcing is based on merging a 0.5° gauge-based data product, the NOAA CPCU (M. Chen et al. 2008), and 2) the Catchment land surface model used in MERRA-Land was updated and now matches that used in the AGCM of the GEOS-5 REDOBS experiment. In replay mode, the land surface model is integrated forward in time with hourly MERRA radiation and near-surface meteorology. Daily CPCU precipitation amounts are disaggregated in time such that the corrected MERRA precipitation matches that from CPCU for daily totals at each 0.5° grid cell. MERRA-Land output is available at a spatial resolution is ⅔° by ½° compared to 1.0° for monthly GLDAS-2 products.

Using an observationally driven empirical approach, the Max Planck Institute for Biogeochemistry (MPI-BGC) ET estimate (Jung et al. 2009, 2010) is diagnostic in nature and employs a machine-learning methodology (model tree ensembles) to up-scale eddy covariance measurements from FLUXNET (Baldocchi et al. 2001) to a 0.5° monthly product. This retrieval, using a surface energy balance constraint, is driven by absorbed photosynthetically active radiation (fAPAR) datasets derived from Sea-Viewing Wide Field-of-View Sensor (SeaWiFS) (Gobron et al. 2007) in conjunction with Advanced Very High Resolution Radiometer (AVHRR) normalized difference vegetation index (NDVI) data (Vermote and Saleous 2006), near-surface air temperature from the University of East Anglia Climate Research Unit, precipitation data from GPCC, and an estimation of the top of the atmosphere shortwave radiation. Though some near-surface reanalysis data and observed precipitation data are used, the resulting ET estimates represent a methodology fundamentally independent from hydrologic model simulations.

c. *Effects of observing system nonhomogeneity*

Throughout the ~30-yr period studied here, the global observing system changes considerably, most dramatically in terms of satellite data observations. To detail all these data stream changes is beyond the scope of this paper and we refer the reader to Figs. 3 and 4 in Rienecker et al. (2011), Fig. 14 and section 4 in Dee et al. (2011), Fig. 4 in Saha et al. (2010), and the related discussion in these papers for details on satellite observations used in the reanalyses. Two specific changes have had notable impacts. The first of these is the beginning of the SSM/I data in July 1987 and the subsequent increase in the number of these sensors to a peak in the mid-1990s. This increase in column water vapor and wind speed information over ocean moistened the MERRA reanalysis and increased precipitation globally (Robertson et al. 2011; Rienecker et al. 2011). For ERA-I, on the other hand, there is some indication that the effect of SSM/I is to *decrease* precipitation. In CFSR near-surface wind speeds are the only retrievals ingested from SSM/I (Saha et al. 2010). A second important change in the data stream is the onset of Advanced Microwave Sounding Unit (AMSU)-A/B availability in Nov 1998. The window channels of this sensor are sensitive not only to near-surface moisture and temperature but also to emissivity-weighted surface temperature; they are assimilated by MERRA and CFSR, but not by ERA-I. MERRA responds with step increases of water vapor and precipitation with these sensors on *NOAA-15* and *-16* (Robertson et al. 2011). Similarly, CFSR moisture analysis increments and $P - E$ values increase as these sensors are introduced (Wang et al. 2011). We consider the implications of these sensor effects on reanalysis moisture transport between land and ocean in section 4.

TABLE 3. Multiplicative coefficients used to intercalibrate SSM/I and SSM/IS (*F17*) global ocean rainfall estimates from various sensors by two different retrieval algorithms using *F13* as the reference sensor for each. Values were determined using temporal overlaps of ocean – averaged precipitation between various sensors.

	F8	*F10*	*F11*	*F13*	*F17*
RSS V7	1.025	1.010	1.03	1.00	1.016
GPROF 2010 V1a	1.00	1.015	1.02	1.00	—

In addition to these reanalysis impacts, direct satellite retrievals of E and P involves the intercalibration of different flight instruments, even of the same type. The accuracy of trends and decadal signals in GPCP, RSS products, OAFlux, and other retrievals depends on spacecraft platforms that have different diurnal sampling times, changes in orbital height and spacecraft attitude, in addition to individual sensor spectral response functions. Inadequate temporal overlap among early SSM/I instruments is also a problem. More details on their likely influence on variability is provided in sections 3 and 4 as we interpret temporal behavior of specific datasets.

3. Remotely sensed *E* and *P* over the global oceans

a. *Ocean precipitation*

Figure 1a shows time series of global ocean averages of the three precipitation estimates in the form of anomalies around their respective monthly climatologies. For both RSS and GPROF we have performed an ad hoc intercalibration of the precipitation from the SSM/I sensors of *F8*, *F10*, *F11*, *F13*, and *F17* by using overlaps in time between sensors and adjusting the offsets relative to *F13*. Even with sensor T_b calibration

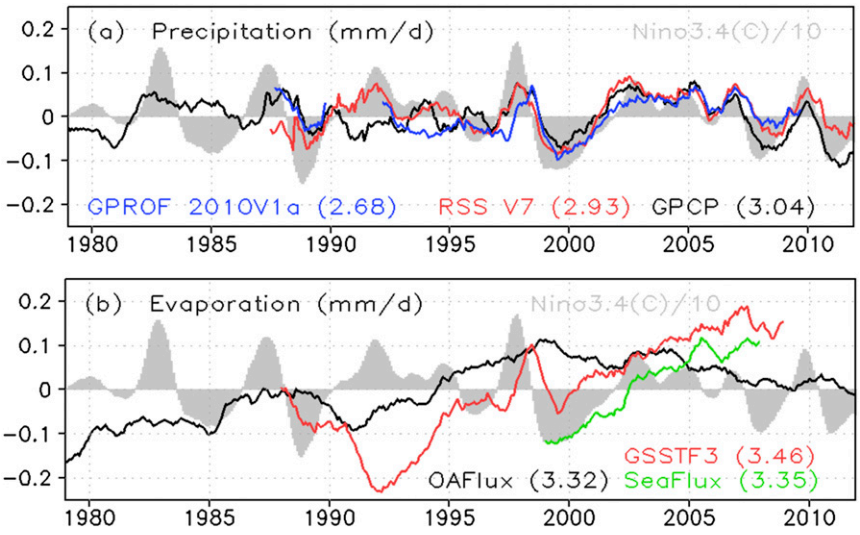

FIG. 1. (a) Ocean area-average precipitation (60°N/S) from GPCP V2.2 (black), RSS V7 (red) and GPROF 2010V1a (blue). Anomalies (mm day^{-1}) are around monthly resolved climatology (annual averages in parentheses). Gray shading is Niño-3.4 SST anomaly. A 13-month running smoother has been applied. The gap in 1990–92 for GPROF 2010 V1a corresponds to a period when the SSM/I 85-GHz channel failed. See text and Table 3 for discussion of how RSS V7 and GPROF 2010 V1a data for individual sensors were intercalibrated. (b) As in (a), but for evaporation: OAFlux (black), GSSTF3 (red), and SeaFlux(green).

improved, twice-a-day sampling and changing orbit equator crossing times can affect P estimates. The multiplicative factors used (Table 3) are of order one percent; however the changes are important since they affect decadal variability of the near-global quantities. Because the 85-GHz channel on *F8* was lost in 1990 and this affects the GPROF algorithm, *F8* data after this date are not used. After these adjustments correlations among the three estimates from 1992 through 2009 are reasonably high: r(RSS, GPCP) = 0.72, r(RSS, GPROF) = 0.80, and r(GPROF, GPCP) = 0.66. Standard deviations of the monthly anomalies for GPCP, RSS, and GPROF are 0.09, 0.11, and 0.09 mm day^{-1}, respectively. All three retrievals show a coherent relationship to Niño-3.4 SST after the mid-1990s. Before that time there is poor agreement between the retrievals, most likely relating to limited periods of overlap for intercalibrating of individual sensors. GPCP also decreases systematically (in a relative sense) compared to the other two estimates after 2005 when *F17* SSM/IS becomes available. The extent to which the transition from *F13* to *F17* is responsible for these differences is now being investigated.

Differences in the climatological means of these algorithms when globally integrated (over ocean) range from 2.68 to 3.04 mm day^{-1}. The most prominent difference is the systematically smaller values of GPROF. In GPROF 2010 V1a the SSM/I rain rates were adjusted to match the TMI V7 within the TRMM region (±37.5° latitude). This relationship may not be appropriate at higher latitudes owing to the preponderance of lighter rainfall rates that the TRMM radar would not adequately detect. Behrangi et al. (2012) used the *CloudSat* cloud profiling radar (CPR), a sensor more sensitive to lighter rainfall rates and more accurate in distinguishing precipitation versus cloud droplet size hydrometeors, to argue that current passive microwave sensors miss substantial fractions of high latitude precipitation. GPCP attempts to counter the high latitude bias by use of low-orbit IR/microwave sounder cloud information. A TRMM composite climatology (Adler et al. 2009) and its input components from various TRMM algorithms [including GPROF applied to TMI and from the TRMM precipitation radar (PR)] confirm the GPCP mean value in the 60°N/S ocean agrees reasonably with Behrangi et al. (2012). Behrangi et al. (2014) provides further support for GPCP values at most latitudes, based on *CloudSat* and other data. Thus, although we are interested mainly in variations of ocean precipitation, the absolute magnitude for this study should be considered roughly that of GPCP, with an error bar of about ±7% for that mean value (Adler et al. 2012).

b. Ocean evaporation

The poor consistency between ocean evaporation estimates (Fig. 1b) stands in contrast to the good agreement among the ocean precipitation estimates (Fig. 1a). The

highest correlation between OAFlux and GSSTF3 is 0.61 during the period 1988–2008 and is largely due to an upward trend in both datasets. During the SeaFlux period (1998–2007) GSSTF and SeaFlux correlate with OAFlux at 0.05 and 0.18, respectively, and actually have trends opposing that of OAFlux. Climatological E values all similar (3.3–3.4 mm day^{-1}) and systematically exceed the largest values for P, implying net climatological transport of moisture to land. Standard deviations of OAFlux, GSSTF3, and SeaFlux monthly anomalies around the climatologies are 0.077, 0.132, and 0.095 mm day^{-1}, respectively.

To better understand the variations among evaporation products, we quantify the relative importance of components affecting the time variation of E in Eq. (1) through a Taylor's series expansion of the bulk formula around the monthly, spatially resolved climatology applied to each of these three datasets at full spatial resolution. Variations in E can be decomposed as

$$\delta E = \underbrace{\overline{\frac{\partial E}{\partial \Delta q}}}_{\substack{\text{Moisture}\\ \text{Deficit}\\ \text{Sensitivity}}} \delta\Delta q + \underbrace{\overline{\frac{\partial E}{\partial U}}}_{\substack{\text{Wind}\\ \text{Speed}\\ \text{Sensitivity}}} \delta U + \underbrace{\overline{\frac{\partial E}{\partial C_E}}}_{\substack{\text{Exchange}\\ \text{Coefficient}\\ \text{Sensitivity}}} \delta C_E. \tag{2}$$

In this formulation monthly resolved climatological quantities (denoted by overbars) represent the climatological sensitivity to changes in moisture deficit, wind speed or the exchange coefficient: $\overline{C_E \rho_a U}$, $\overline{C_E \rho_a \Delta q}$, and $\overline{\rho_a U \Delta q}$. They vary in space and with calendar month. We estimated wind speed effects on the turbulent exchange coefficient using the C_E formulation of Bentamy (2003). Global averages of these linearized interactions (sensitivities multiplied by the appropriate monthly anomalies of wind speed, Δq, and exchange coefficient) indicate how those quantities contribute to net E variations. These sensitivities retain spatial structure so that the terms are not just a constant scaling of global mean U, Δq, or C_E anomalies.

Deconstructions of E variability for each of the three datasets are shown in Fig. 2. All quantities are anomalies around the respective monthly climatologies for each dataset. For reference we show anomalies of *global* ocean SST instead of Niño-3.4 since the former relates directly to changes in q_s through the Clausius–Clapeyron relationship. OAFlux (Fig. 2a) shows a steady rise in E until 2000 and then declines thereafter. Both wind speed and Δq changes are important contributors to E variability with correlations near 0.80. On longer time scales wind increases prior to 2000 play a prominent role in OAFlux E increases (Yu 2007). This long-term wind speed increase is also reflected in sea level height fluctuations across the Pacific basin during the 1990s (Merrifield et al. 2012). E declines after 2000 are also strongly affected by Δq decreases, possibly reflecting the propensity for more persistent cold tropical SST states associated with the shift in the phase of the PDV. Variations in the exchange coefficient are very small and typically at least an order of magnitude smaller than the other terms. On interannual time scales, one can see that wind and Δq contributions are weakly anticorrelated. This relationship is likely a signature of equatorial wind stress – SST anomaly feedback associated with El Niño events. Early in the evolution of a warm SST event, the strong equatorial easterlies collapse. At the same time q_s values are increasing in the eastern equatorial Pacific due in part to relaxed equatorial upwelling of cold water and the subsequent increase of near surface vertical moisture gradient.

GSSTF3 (Fig. 2b) shows much greater intensification of E during the common period with increases of 0.40 mm day^{-1} from 1992 to 2006 compared to about 0.15 mm day^{-1} for OAFlux. Though both winds and thermodynamic changes contribute to the strong upward E trend it is the Δq values that largely drive the difference. Compared to OAFlux, GSSTF3 Δq contributions to E follow SST anomalies much more closely—note for example the early 1990s where OAFlux values are nearly flat but GSSTF3 excursions reach −0.15 mm day^{-1}. Since q_s anomalies should mirror SST changes (though nonlinearly) this indicates substantial q_a differences in the two datasets. The anticorrelation between Δq and wind speed contributions to E on shorter time scales is even more pronounced in GSSTF3. Wind speed contributions decrease (Δq contributions increase) as the 1997 El Niño event begins. Opposite behavior is present for the succeeding cold event at the turn of the century. SeaFlux (Fig. 2c) exhibits a similar strong upward E increase of 0.20 mm day^{-1} over its shorter 10-yr period. The Δq term is again the largest driver with SeaFlux but the wind contribution is almost as big.

Significant differences in wind speed estimates feeding into the various E calculations are present at near decadal scales (Fig. 3). All datasets capture the large drop in wind speeds in 1990–1992 during the transition to El Niño conditions. The onset of this warm event follows the eruption of Mt. Pinatubo in mid-1991 (Trenberth and Dai 2007; Wisser et al. 2010). The precipitous decline of wind speed prior to the 2009/10 El Niño is also apparent in OAFlux, CCMP, and RSS V7. For the entire period, RSS V7 retrievals have the largest absolute values but there are some important relative

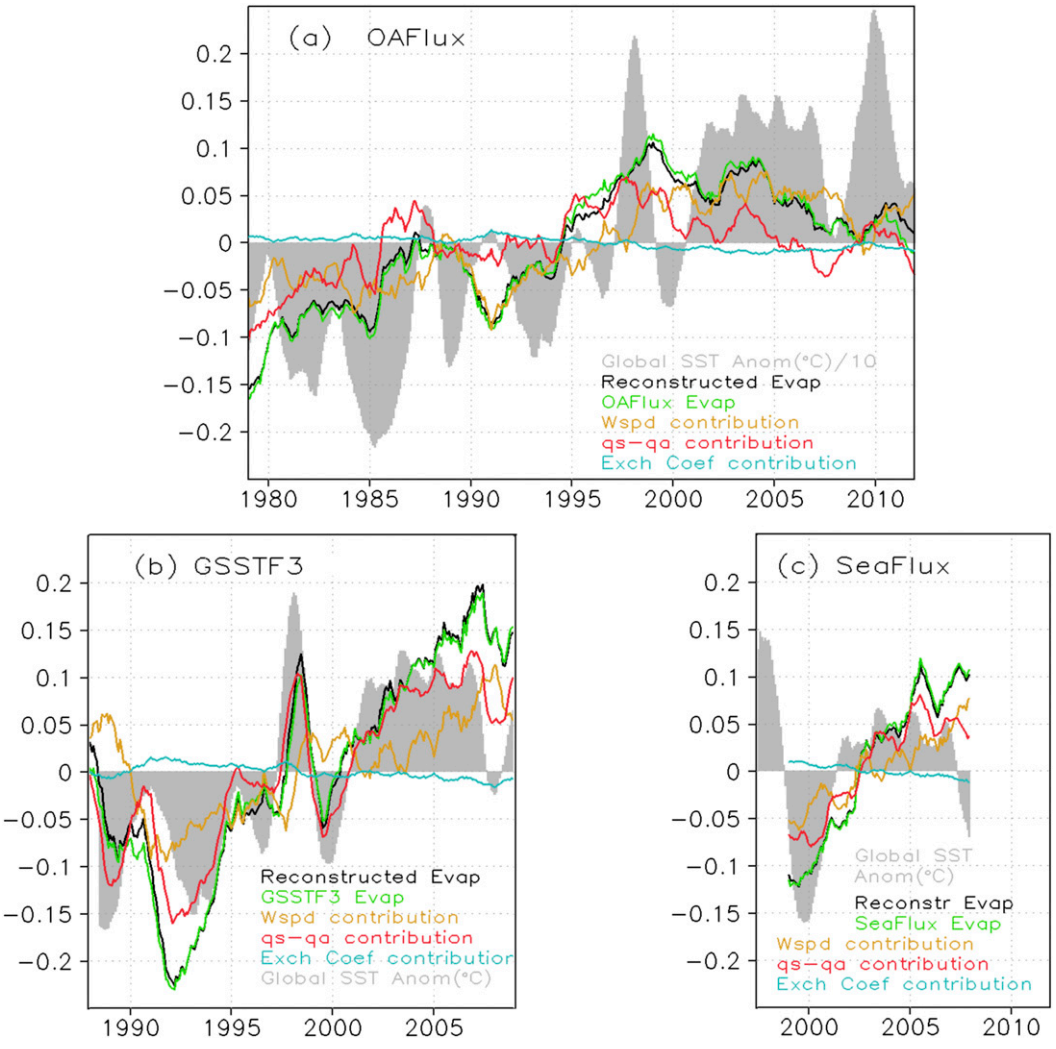

FIG. 2. Global mean ocean area averaged (60°N/S) evaporation rate anomalies (green curves, mm day^{-1}) for (a) OAFlux, (b) GSSTF3, and (c) SeaFlux. Shaded areas are global SST anomalies. Anomalies are around the respective climatological annual cycles. Also shown are contributions to the anomalies by wind speed (yellow), $q_s - q_a$ (red), and the exchange coefficient (cyan). Recovery of the total E signal using the decomposition in Eq. (2) in the text is shown by the black curves.

differences with other datasets. GSSTF3 has a steeper increase in speed between 1990 and 2007, due likely to the inclusion of other SSM/I sensors (e.g., *F14* and *F15*) that drift through the diurnal cycle. Also, the relative minimum in RSS V7 winds in the early 1990s is not so prominent as in the other datasets and likely results from better calibration of the *F11* sensor in V7 compared to V6. CCMP and SeaFlux show increased wind speeds during the early 2000s, but they have a relatively flatter change over the 1998–2001 period while OAFlux, RSS V7, and GSSTF3 winds all indicate a decrease. Other the other hand, OAFlux wind speed levels off after the early 2000s in contrast to a continued rise in RSS V7. One can anticipate from Fig. 2 that, should these RSS V7 wind speeds be adopted for use in E retrievals, there could be nonnegligible changes.

c. *Ocean $E - P$ synthesis*

Resulting $E - P$ estimates made by various combinations of these products (Fig. 4) show considerable differences in variability. Here we have again removed the climatological mean and annual cycle from each product. OAFlux-based $E - P$ estimates show essentially no increases after 2000 in contrast to GSSTF, which increases sharply after 2002. SeaFlux-based $E - P$ during the shorter 1998–2007 period indicates E increases of nearly 0.20 mm day^{-1}. So only the OAFlux-based $E - P$ estimates suggest a relative maximum in

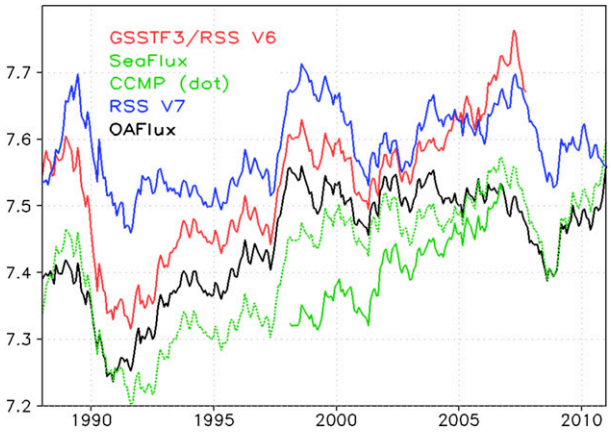

FIG. 3. Wind speed ($m\,s^{-1}$) over the global oceans (60°N/S) for RSS V7 (blue), OAFlux (black), GSSTF3/RSS V6 (red), SeaFlux (green solid), and CCMP (green dotted). A 13-month running smoother is applied.

$E - P$ near 2000. The choice of P does not materially alter this result. Despite these differences in lower frequency signals, interannual variations seem reasonably coherent, except perhaps before the mid-1990s.

Several important changes in OAFlux blending of reanalysis and remote sensing retrievals should be noted. In 2000 the Chou et al. (1995) satellite estimates of q_a change to those of Jackson et al. (2009). MERRA near-surface meteorology also replaces that of 40-yr ECMWF Re-Analysis (ERA-40) after the latter ends in 2002. Finally, the RSS V7 SSM/IS winds replace the V6 SSM/I winds after December 2006. Differing bias properties of these input data are accounted for using buoys as reference (Yu et al. 2008), but the sparse coverage of the buoys is an issue. In OAFlux, decreasing Δq after 2000 is actually the major forcing for producing the decrease in E (Fig. 2a). In contrast, Δq in GSSTF3 and SeaFlux help drive E increases beyond the turn of the century. That this OAFlux Δq decrease occurs during important changes to input data streams invites more critical analysis. Another issue is the sensitivity of $E - P$ variations to alternative wind retrievals. A simple estimate of the effect of the RSS V7 wind speeds (Fig. 3) can be made by scaling OAFlux E by the ratio of V7 to OAFlux wind speed and again subtracting off the average of GPCP and RSS V7 P. The result (blue line in Fig. 4) is a much flatter time series with a reduced trend. The $E - P$ variations now also have a more coherent inverse relationship to those of Niño-3.4. Unfortunately, this satellite-derived winds only product can be made just from 1987 onward. In summary, although the interannual ENSO-related $E - P$ signals have reasonable coherence among these estimates we conclude that, for existing datasets, variability of decadal length or longer is likely distorted and remotely sensed estimates do not yet have the accuracy needed over the global oceans.

4. Constraints over global land

a. *Reanalysis vertically integrated moisture convergence*

VMFC estimates from the three reanalyses considered here exhibit strong consistency in their interannual signals (Fig. 5, top) with r(ERA-I, CFSR) = 0.85, r(ERA-I, MERRA) = 0.83, and r(CFSR, MERRA) = 0.88. Standard deviations for ERA-I, CFSR, and MERRA are 0.12, 0.11, and 0.13 $mm\,day^{-1}$, respectively. However, the spread between CFSR and MERRA or ERA-I climatological means is roughly 0.15 $mm\,day^{-1}$, which is large compared to their mean climatological amounts. The global influence of ENSO is apparent with decreases in moisture transports to land during warm events (e.g., 1982/83, 1986/87, 1991/92, 1997/98, and 2009/10). The 1991/92 event represents combined forcing from the warm SST and the effects of Mt. Pinatubo eruption resulting in

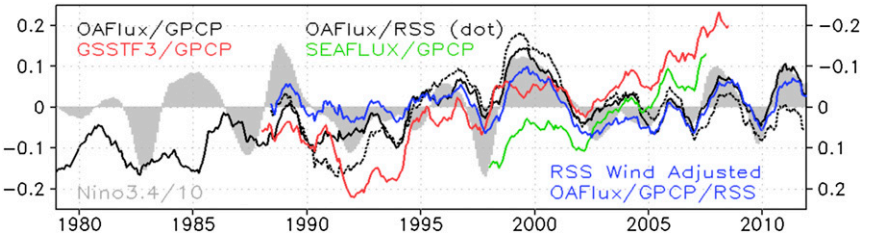

FIG. 4. Global ocean (60°N/S) $E - P$ anomalies ($mm\,day^{-1}$) made from various combinations of datasets. Estimates use OAFlux (black), GSSTF3 (red), and SeaFlux (green) evaporation. OAFlux/GPCP/RSS estimates (blue) replace the OAFlux winds with those from RSS V7 winds and use the simple average of GPCP and RSS V7 precipitation. In all cases the E and P anomalies making up a calculation are made with respect to the climatology extending over the shortest time span. Note that the Niño-3.4 index (shaded gray) is plotted using the reversed scale on the right.

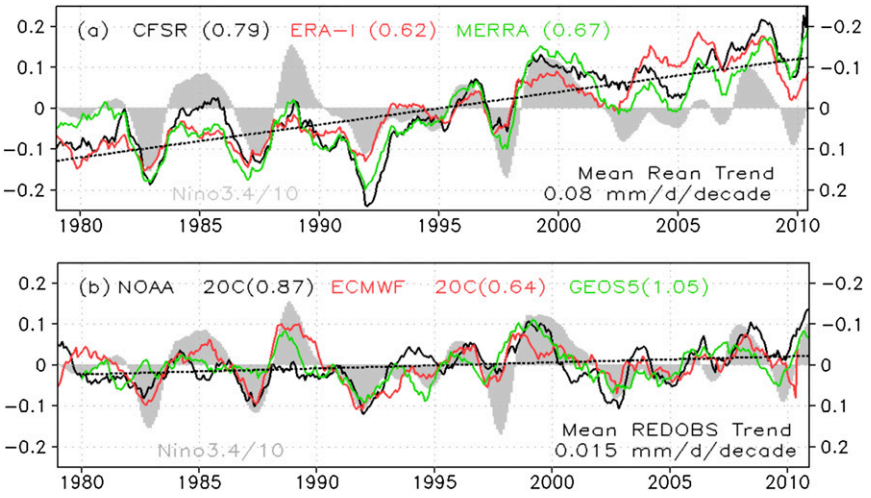

FIG. 5. (a) Global land (60°N/S) vertically integrated moisture convergence anomalies, VMFC, (mm day^{-1}) from MERRA (green), ERA-I (red), and CFSR (black). Climatological values are in parentheses. A 13-month running smoother applied. Note that the Niño-3.4 index (shaded gray) is plotted using the reversed scale on the right. (b) Same as for (a) but using NOAA 20CR (black) "reduced observation" run assimilating only surface pressure and specified SST and ECMWF 20CM (red) and NASA GEOS-5 F25c72 (green) AMIP integrations using only specified SST. Trends were calculated from the average of the monthly reanalysis/model anomalies before smoothing was applied.

a cooling of global land and anomalously low precipitation over tropical continents (Trenberth and Dai 2007; Wisser et al. 2010). Increased transport to land is apparent in cold SST events, the most notable being during the extended late 1998/2000 period.

The trends of the three reanalyses average 0.08 mm day^{-1} decade^{-1}. Most of this upward trend arises after the early 1990s. Robertson et al. (2011) have documented MERRA sensitivity to the additions of SSM/I (July 1987) and particularly AMSU-A (November 1998) data as responsible for spurious P increases (E decreases), especially over ocean. Other reanalyses all share this sensitivity to some degree (Trenberth et al. 2011) and it is likely that much of the upward trend in the reanalysis VMFC over land remains due to these satellite sensor changes.

To test this idea we examined VMFC over land from the three REDOBS analyses: the NOAA 20CR and ECMWF 20CM and NASA GEOS-5 F25c72 Atmospheric Model Intercomparison Project (AMIP) model simulations using data from the same 30-yr period. Recall that the NOAA 20CR integrations are forced with observed SST and surface pressure observations while the AMIP-style integrations have only SST forcing. The REDOBS experiments are essentially free of significant observing system changes while retaining the ability to respond to SST influences on the atmospheric water budget. Comparing Fig. 5a to Fig. 5b the REDOBS experiments exhibit trends systematically much weaker (0.014 mm day^{-1} decade^{-1}) compared to the full reanalyses (0.08 mm day^{-1} decade^{-1}). These integrations also retain a considerable amount of the interannual signal associated with ENSO events as seen in the full reanalyses. Although the climatology in each of the models is biased in some way, the systematically much smaller REDOBS VMFC anomaly trends strongly suggest that the major upward trends in the full reanalyses are data assimilation artifacts related to observing system changes.

b. *Land surface modeling and diagnostic evapotranspiration datasets*

Given that we expect anomalous moisture transport to land to agree with $P - \mathrm{ET}$ there, we turn now to an examination of the offline LSMs, their P forcing and resulting ET (Fig. 6). (To facilitate the comparison, in this plot P and E are shown including their climatological time mean values and not as anomalies.) Also plotted is the global land time series of GPCP V2.2 that updates the version 2.1 used in the Princeton forcing. Mean values of the precipitation forcing range from about 2.0 to over 2.5 mm day^{-1}. The GPCC analysis, to which GPCP anchors, now uses an analysis technique that establishes gauge climatologies and then determines monthly anomalies in the V6 full and V4 monitoring analyses. This has elevated the mean between GPCP V2.1 and V2.2 because of a better analysis in mountainous areas. GPCP also uses a seasonally

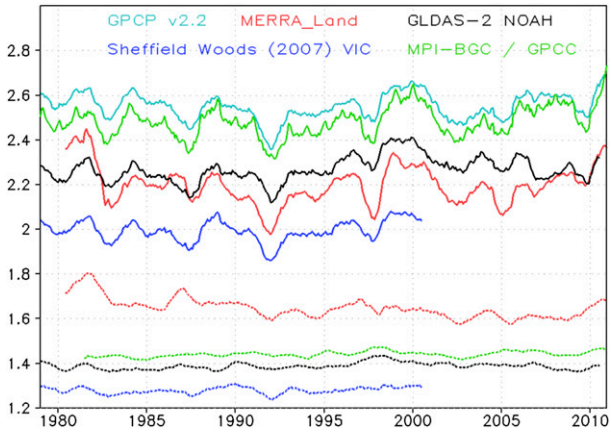

FIG. 6. Precipitation forcing (solid lines) and derived evapotranspiration (dashed lines) from three offline land data assimilation efforts over land (60°N/S) for MERRA-Land (red), GLDAS-2 Noah model (black), and Sheffield and Wood (2007). Also shown is ET derived from the MPI-BGC diagnostic biophysical retrieval and GPCC V6 precipitation. The mean climatological annual cycle has been removed from each time series and a 13-month smoother applied.

varying wind loss adjustment that always increases precipitation, significantly so in cold months. These adjustments are not present in the CPCU dataset that was used in MERRA-Land, nor does CPCU use satellite information to help interpolate between gauges in sparsely monitored regions. Despite disagreement in mean values, interannual precipitation variability is consistent between CPCU and the other estimates. Precipitation over land is reduced during El Niño years (e.g., 1982/83, 1986/87, 1992, 1997/98, and 2009/10) in association with enhanced moisture convergence over warmer tropical oceans (Gu et al. 2007). There is some evidence of a downward trend in precipitation during the 1980s prior to the low-frequency minimum coinciding with the 1991/92 El Niño and the Pinatubo volcano event in mid-1991 (Trenberth and Dai 2007; Wisser et al. 2010).

The ET time series (shown by the dashed lines in Fig. 6) have far less interannual variability, likely a result of solar forcing exerting additional control over moisture availability and the integrative nature of soil moisture in response to precipitation. Three estimates, GLDAS-2 Noah, VIC, and MPI-BGC, are clustered at values near 1.2–1.4 mm day^{-1}. This range of values is consistent with the Mueller et al. (2013) ET estimate of 1.35 mm day^{-1} for all datasets considered, including the reanalyses.[2] MERRA-Land ET is about 0.25 mm day^{-1} larger than for Noah, even though MERRA-Land precipitation averages about 0.05 mm day^{-1} less than that of Noah. The elevated ET in MERRA-Land can be traced back to the even higher ET in the standard MERRA output. The latter can be attributed to excessive rainfall interception by and reevaporation from the vegetation canopy, which has been fixed in MERRA-Land (Reichle et al. 2011, their Fig. 4), and to elevated net radiation at the surface, which for MERRA-Land is about 7 W m^{-2} (~0.25 mm day^{-1}) higher than for Noah. The downward trend in MERRA-Land ET prior to the mid-1990s is also at odds with many other models, although it is consistent with the CPCU precipitation used in MERRA-Land. Mueller et al. (2013) found a mean ET increase of 0.03 mm day^{-1} decade^{-1} over the period 1989–2005 for all datasets considered, though this is strongly influenced by positive contributions from reanalyses making up the database used in that study. More specifically, they find increases prior to 1997, but decreases or steady values thereafter. This result is also characteristic of the MPI-BGC ET dataset (Fig. 8 in Jung et al. 2010) as well as another recent satellite derived ET estimate not shown here (Yao et al. 2012).

Three resulting P − ET anomaly time series are displayed in Fig. 7a. The MPI-BGC ET was combined with the GPCC precipitation, which was a referencing dataset for the ET diagnosis. Correlations among three estimates are uniformly high: r(MERRA-Land, GLDAS-2 Noah) = 0.77, r(MERRA-Land, MPI-BGC/GPCC) = 0.86, and r(MPI-BGC/GPCC, GLDAS-2 Noah) = 0.76. Standard deviations for GLDAS-2 Noah, MPI-BGC/GPCC and MERRA are 0.11, 0.12, and 0.12 mm day^{-1}, respectively. The P − ET for these analyses also reflects the dominant ENSO-related forcing of interannual variations of the precipitation; correlation of the mean LSM anomalies with the Niño-3.4 index is 0.79. Yet, a large intermodel climatological bias is also present originating from the precipitation component.

The overall agreement between reanalyses, their reduced observation counterparts, and LSMs is assessed in Fig. 7b. LSM and REDOBS trends agree much better with each other than they do with the full reanalyses. The trend of the mean of the LSMs P − ET, 0.024 mm day^{-1} decade^{-1}, is significant at the 99% level but the reduced observation reanalyses trend, 0.013 mm day^{-1} decade^{-1} (Fig. 5b) is only significant at the 90% confidence level. (Lag 1 autocorrelation of the P − ET time series was used to determine the number of independent observations—typically about one-third of the time series length.) The similarity in LSM and REDOBS trends, their difference from that of the reanalyses, and their mutual independence strongly support our contention that the large

[2] For the MPI-BGC ET data we have assigned values of zero to areas where estimates are not retrieved over the Sahara desert so as to be consistent with LSMs which solve for ET in this region. This reduces the global mean ET value by about 0.12 mm day^{-1} because of the enlarged averaging region.

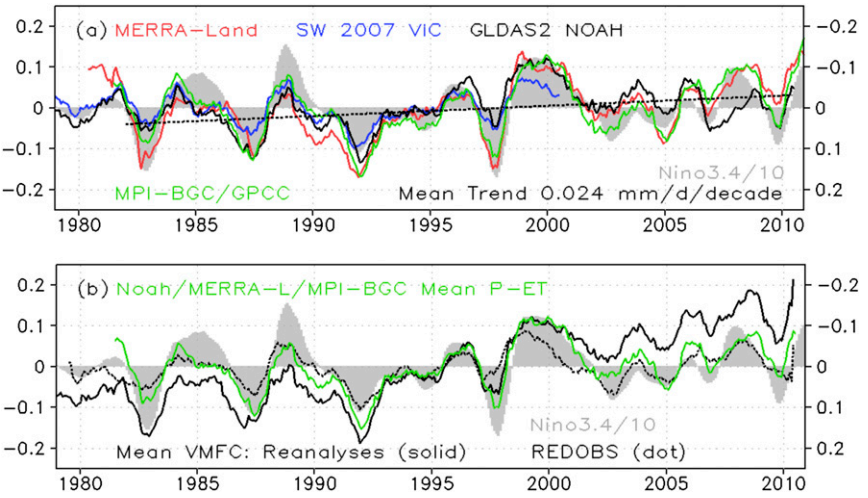

FIG. 7. (a) Global land (60°N/S) $P - \mathrm{ET}$ anomalies for each of the LSMs. The trend was calculated from the average of the monthly reanalysis/model anomalies before smoothing was applied. Note that the Niño-3.4 index (shaded gray) is plotted using the reversed scale on the right. (b) Global land (60°N/S) ensemble mean LSM $P - \mathrm{ET}$, reanalysis VMFC, and REDOBS VMFC (mm day^{-1}). All units are mm day^{-1}. A 13-month running smoother is applied.

reanalysis trends are spurious. In section 5 we interpret the LSM trends as possible signatures of decadal fluctuations of ENSO frequency and amplitude.

5. Discussion

Drawing together these results, the largest uncertainty lies in remotely sensed ocean $E - P$ variability (Fig. 4) and is driven primarily by the pronounced differences in E variability from GSSTF3 and SeaFlux with OAFlux. Satellite determinations of both near surface humidity and wind speed contribute to these differences. Significant differences in the winds going into the evaporation retrievals have been noted (Fig. 3). The RSS V7 are likely the most consistently intercalibrated dataset over the SSM/I and SSM/IS era. Nevertheless, lack of sampling at times other than near 0600 and 1800 local equatorial crossing times may affect their mean values. These new winds have not yet been incorporated in evaporation retrievals, though the exercise of approximating OAFlux wind speeds with RSS values improves the relationship of resulting $E - P$ to Niño-3.4 SST variations. Uncertainties in q_a are a bigger challenge given the indirect relationship of 2-m humidity retrievals with the coarse vertical moisture structure inherent with passive microwave data. The divergence of q_a values between OAFlux and GSSTF3 (and SeaFlux) after about 2000–02 is a key uncertainty since it occurs during a period where SSTs are emerging from a pronounced cool period. Unfortunately, OAFlux also changes to a different satellite retrieval algorithm source for q_a and reanalysis near-surface meteorology near this time. We suspect that cloud water contamination, or even biasing observations toward cloud free areas may have degrading effects on passive microwave q_a retrievals.

Precipitation estimates over ocean are not without problems as we noted, due in part to the uncertainty in the contribution of numerous but light precipitation events in higher latitudes and in subtropical ridges. Temporal sampling variations along the time record of the SSM/I suite and equatorial crossing time drifts might still contribute to the fine details of the intercalibration stability of the times-series. Prior to late 1987 there is no passive microwave precipitation measurement and the GPCP strategy of calibrating IR measurements becomes less direct and more problematic. Moreover, intercalibration of *F8* with other SSM/I sensors is hampered by poor temporal overlap with *F10* and *F11*. Though the relative uncertainties in ocean P are less than those of E, the intercalibration efforts remain a work in progress and the precipitation record before the early 1990s needs additional scrutiny.

Comparison of LSM $P - \mathrm{ET}$ and the VMFC diagnostics from reanalyses and REDOBS provides considerable insight linking direct near-global land water balance variations to those over ocean. Good agreement on *interannual time scales* between these three approaches and correlations with Niño-3.4 underscore the first order influence of ENSO in governing ocean–land moisture exchange, consistent with the results of Gu et al. (2007) and Syed et al. (2010). However, the strong upward trend over the near 30-yr record in the reanalyses is not shared by the LSMs or the REDOBS.

Formally, VMFC from the full reanalyses is independent of the LSMs since the latter are run in offline mode or diagnostically while the reanalyses depend on analyzed state variables of wind and moisture. Some indirect links do exist though through the radiative forcing and near-surface meteorology in the LSM results since they are influenced to varying degrees by the atmospheric reanalyses. REDOBS differences with the reanalyses are largely of a trend nature and can be cleanly interpreted as due to observing system changes affecting the latter. The good agreement on lower frequency behavior between REDOBS and LSMs effectively narrows the uncertainty on water balance variations over land during the satellite era.

By virtue of Green's theorem flux divergence of moisture must vanish globally, so with the additional knowledge that atmospheric moisture storage changes are small on these scales, the land $P - ET$ also constrains $E - P$ over oceans. So the substantial scatter in ocean $E - P$ estimates in Fig. 4 compared to the LSM results in Fig. 7a and the much better agreement between LSMs and REDOBS in Fig. 7b emphasizes the current challenges in direct $E - P$ retrievals over ocean. (Note that to quantify this comparison, the values in Fig. 7 have to be reduced by a factor 1/2.3 to account for the ratio of ocean to land fraction within the 60°N/S latitude band.) Given the uncertainty in ocean E variability we make an alternative calculation as follows: We take land $P - ET$ (or, equivalently, VMFC) values from the LSMs and scale the resulting time series values by 1/2.3 to get the equivalent $E - P$ over ocean, with the implicit but reasonable assumption that atmospheric storage variations are negligible. Then either the GPCP or RSS V7 precipitation is added to recover E as a residual. This calculation (Fig. 8) obviously collects errors from each of the input P and ET datasets, including absolute biases. Despite this accumulation of uncertainty the residual calculation strongly suggests that the GSSTF3, SeaFlux, and likely other current satellite-only estimates are outliers in terms of decadal-scale E variations. Furthermore, evidence supporting a pronounced E decline after the late 1990s as in OAFlux is rather weak. In an area-averaged sense ocean P (Fig. 1a) and land $P - ET$ variations (Fig. 7b) have approximately the same amplitude. But in accounting for the fractional area of land to ocean [land $(P - ET)/2.3$] for the 60°N/S band, the character of the ocean P variability strongly influences our inference of E. The results emphasize that because of the significant cancellation between E and P over ocean, obtaining accurate global ocean $E - P$ and inferring VMFC from remote sensing methods alone remains a challenge. Clearly, these diagnostics are not definitive but they are another way of underscoring the current uncertainty in E variability as well as the need to revisit sources of error in P estimates.

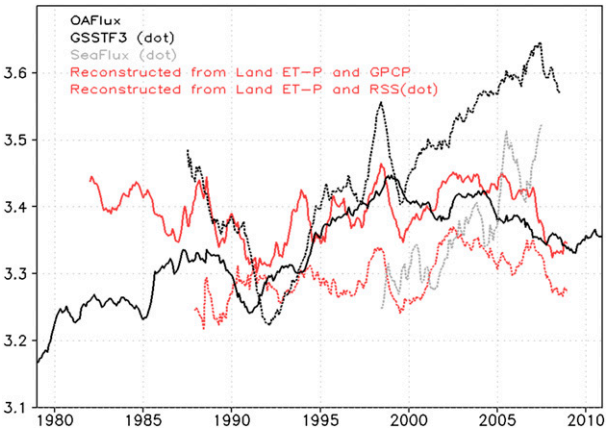

FIG. 8. Various reconstructions (red) of ocean area-average evaporation. Reconstructions are diagnosed by scaling mean LSM $P - ET$ by 1/2.3 to account for the relative fractions of land and ocean in the 60°N/S band, and then adding either GPCP or RSS V7 precipitation to recover ocean evaporation. OAFlux, GSSTF3, and SeaFlux ocean evaporation are also shown for comparison. All units are mm day^{-1}.

Returning to the question whether different combinations of datasets provide evidence of a recent climate shift, we see suggestive but conflicting evidence. OAFlux-based ocean $E - P$ estimates (Figs. 5 and 8) clearly indicate a relative maximum around 1999/2000. But as we noted earlier, the strength of this maximum is subject to uncertainty in terms of changing OAFlux input data streams after this point. The potential reduction in the wind speed trend from RSS V6 to V7 could act to increase E in the early to mid-1990s, reducing the relative amplitude of the E maximum and $E - P$ estimates shown in Fig. 4. On the other hand the $P - ET$ estimates from observationally driven LSMs also show the 1999/2000 maximum, around which the character of ENSO-related variations change. Before this time $P - ET$ events associated with warm ENSO events are more strongly negative. However, over the last decade these warm events tend to be of smaller amplitude. This behavior contributes to the upward $P - ET$ trend of the mean LSM signal (Fig. 7b). There is much speculation regarding the possible change of El Niño type and the increase of so-called "central Pacific" versus "eastern Pacific" events (Ashok et al. 2007; Kao and Yu 2009) over recent decades. McPhaden et al. (2011) have related the relative change in El Niño type occurrence after 2000 to changes in the background ocean state, manifest as a cooling of the eastern tropical Pacific and flattening of the east–west ocean thermocline slope. This is consistent with the studies cited earlier pointing to a recent phase shift in the PDV from various diagnostic perspectives (Burgman et al. 2008; J. Chen et al. 2008; Gu and Adler

2013; Lyon and DeWitt 2012; Lyon et al. 2013). Because of the global land–ocean perspective used in this study we suspect that the ''climate shift'' (or change in the PDV phase) is manifest more subtly as the small trend in LSM $P - ET$, induced by the less pronounced focusing of VMFC over ocean that has characterized warm events predominant since 2000.

6. Concluding remarks

Motivated by the question of whether recent indications of interannual to decadal climate variability and a possible climate shift may have affected the global water balance, we have examined $E - P$ variability integrated over the global oceans and global land from three points of view—remotely sensed retrievals and syntheses over the oceans, reanalysis vertically integrated moisture convergence over land, and offline land surface and diagnostic biophysical models forced with precipitation, radiation, and near-surface meteorology. Our results highlight significant satellite retrieval uncertainties in ocean evaporation and call for additional work to understand weather regime dependencies in q_a. Current precipitation time series over ocean show no large long-term trend but still need work to improve interannual to decadal variations. Further analysis of high latitude ocean rainfall from *CloudSat* and the Global Precipitation Measurement (GPM) mission, with its dual-frequency precipitation radar should clarify precipitation algorithm uncertainty sources. There is clearly work to be done, however, to improve the credibility of multisensor decadal and longer time series. In particular, large differences between ocean evaporation time series and issues such as consistent use of EIA information with T_b data emphasize the need for improved communication within the retrieval community as well as a focus on the impact of calibration and other sensor-dependent issues on the retrievals.

Similarly, more attention to errors related to observing system changes is needed to improve reanalyses and LSMs. Evidence for spurious trends in reanalyses is compelling and more analysis of their origin, regional details, and methods to remove them is needed. Furthermore, we would argue that reduced observations experiments are an essential complement to any reanalysis effort as they help quantify spurious signals arising from observing system changes. Under the auspices of the Global Energy and Water Cycle Experiment (GEWEX) Radiation Panel, the LandFlux initiative is performing an evaluation of the global ET estimates obtained from diagnostic models, constrained LSMs, and global reanalyses (e.g., Jimenez et al. 2011; Mueller et al. 2011, 2013). These initial assessments show that differences in model results can originate both in forcing data and in model configuration. This diversity is evident in our diagnostics and we believe that additional involvement of the climate variability community with LandFlux is warranted.

As expected, our work with reanalyses and LSMs underscores the significant controls that tropical SST variations exert on land ocean moisture transport. While the global land averaging process smears out regional details we believe that LSM $P - ET$ variations before and after the 1997/8 El Niño and their correspondence to those in Niño-3.4 variability are signatures of changes in PDV phase centered around this date. The variability in climate signals, both interannual and longer, obviously has important regional expression that we have not addressed and which is a next step in this research. Algorithm uncertainties and biases are expected to have regional and situational or regime dependence. Furthermore, radiative fluxes and heat balance variations that are tightly coupled to the water cycle have not been addressed. Improved energy budget closure during the tenure of the Clouds and the Earth's Radiant Energy System (CERES) instrument starting in 2000 will be reported soon (T. L'Ecuyer et al. 2014, unpublished manuscript). But for the purposes of determining decadal variations, linkage with earlier Earth Radiation Budget Experiment (ERBE) era measurements starting in 1984 is still work in progress. Improving water and energy fluxes to the accuracy and consistency necessary to adequately determine their role in climate variability over the past few decades remains a challenge.

Acknowledgments. The NASA Energy and Water Cycle Study (NEWS), Dr. Jared Entin, program manager, provided funding for this work. NEWS has been instrumental in encouraging cross-collaborative interactions both internal and external to the investigator team. The authors gratefully acknowledge discussions with numerous individuals, both data providers and users, whose suggestions and clarifications have added substantially to the paper. These include Chung-Lin Shie and Matt Rodell, NASA Goddard Space Flight Center; Lisan Yu and Carol Anne Clayson, Woods Hole Oceanographic Institution; Carl Mears and Kyle Hilburn of Remote Sensing Systems, Inc.; and Martin Jung and Markus Reichstein, Max Plank Institute for Biogeochemistry. The comments of three anonymous reviewers added significantly to this manuscript.

Many of the datasets used in this effort were acquired as part of the activities of NASA's Science Mission Directorate, and are archived and distributed by the Goddard Earth Sciences (GES) Data and Information Services Center (DISC). This included datasets for MERRA, GLDAS, GPCP, and GSSTF3. A number of

other institutions host key datasets: Ocean turbulent heat fluxes and related quantities were obtained from WHOI/OAFlux, http://oaflux.whoi.edu/. RSS (http://www.ssmi.com/) provided ocean precipitation and wind speeds, GPROF rainfall was provided by the CSU Precipitation Research Group (http://rain.atmos.colostate.edu/), global *P* and ET were obtained from the Princeton, University Terrestrial Hydrology research Group (http://hydrology.princeton.edu/). The Max Plank Institute for Biogeochemistry, Biogeochemical Integration Department (https://www.bgc-jena.mpg.de/bgi) supplied satellite-based ET estimates. Vertically integrated moisture flux convergence fields were obtained from the National Center for Atmospheric Research Climate Analysis Section data holdings (http://www.cgd.ucar.edu/cas/catalog/newbudgets/index.html).

REFERENCES

Adler, R. F., and Coauthors, 2003: The version 2.1 Global Precipitation Climatology Project (GPCP) monthly precipitation analysis (1979–present). *J. Hydrometeor.,* **4,** 1147–1167, doi:10.1175/1525-7541(2003)004<1147:TVGPCP>2.0.CO;2.

——, J.-J. Wang, G. Gu, and G. J. Huffman, 2009: A ten-year tropical rainfall climatology based on a composite of TRMM products. *J. Meteor. Soc. Japan,* **87A,** 281–293, doi:10.2151/jmsj.87A.281.

——, G. Gu, and G. J. Huffman, 2012: Estimating climatological bias errors for the Global Precipitation Climatology Project (GPCP). *J. Appl. Meteor. Climatol.,* **51,** 84–99, doi:10.1175/JAMC-D-11-052.1.

Ashok, K., S. K. Behera, S. A. Rao, H. Weng, and T. Yamagata, 2007: El Niño Modoki and its possible teleconnection. *J. Geophys. Res.,* **112,** C11007, doi:10.1029/2006JC003798.

Atlas, R., R. N. Hoffman, J. Ardizzone, S. M. Leidner, J. C. Jusem, D. K. Smith, and D. Gombos, 2011: A cross-calibrated, multiplatform ocean surface wind velocity product for meteorological and oceanographic applications. *Bull. Amer. Meteor. Soc.,* **92,** 157–174, doi:10.1175/2010BAMS2946.1.

Baldocchi, D., and Coauthors, 2001: FLUXNET: A new tool to study the temporal and spatial variability of ecosystem-scale carbon dioxide, water vapor, and energy flux densities. *Bull. Amer. Meteor. Soc.,* **82,** 2415–2434, doi:10.1175/1520-0477(2001)082<2415:FANTTS>2.3.CO;2.

Barlow, M., S. Nigam, and E. H. Berbery, 2001: ENSO, Pacific decadal variability, and U.S. summertime precipitation, drought, and stream flow. *J. Climate,* **14,** 2105–2128, doi:10.1175/1520-0442(2001)014<2105:EPDVAU>2.0.CO;2.

Baumgartner, A., and E. Reichel, 1975: *The World Water Balance*. Elsevier, 179 pp.

Becker, A., P. Finger, A. Meyer-Christoffer, B. Rudolf, K. Schamm, U. Schneider, and M. Ziese, 2013: A description of the global land-surface precipitation data products of the Global Precipitation Climatology Centre with sample applications including centennial (trend) analysis from 1901–present. *Earth Syst. Sci. Data,* **5,** 71–99, doi:10.5194/essd-5-71-2013.

Behrangi, A., M. Lebsock, S. Wong, and B. Lambrigtsen, 2012: On the quantification of oceanic rainfall using spaceborne sensors. *J. Geophys. Res.,* **117,** D20105, doi:10.1029/2012JD017979.

——, G. Stephens, R. F. Adler, G. J. Huffman, B. Lambrigtsen, and M. Lebsock, 2014: An update on oceanic precipitation rate and its zonal distribution in light of advanced observations from space. *J. Climate,* **27,** 3957–3965, doi:10.1175/JCLI-D-13-00679.1.

Bentamy, A., K. B. Katsaros, A. M. Mestas-Nuñez, W. M. Drennan, E. B. Forde, and H. Roquet, 2003: Satellite estimates of wind speed and latent heat flux over the global oceans. *J. Climate,* **16,** 637–656, doi:10.1175/1520-0442(2003)016<0637:SEOWSA>2.0.CO;2.

Burgman, R. J., A. C. Clement, C. M. Mitas, J. Chen, and K. Esslinger, 2008: Evidence for atmospheric variability over the Pacific on decadal timescales. *Geophys. Res. Lett.,* **35,** L01704, doi:10.1029/2007GL031830.

Chen, J., A. D. Del Genio, B. E. Carlson, and M. G. Bosilovich, 2008: The spatiotemporal structure of twentieth-century climate variations in observations and reanalyses. Part II: Pacific pan-decadal variability. *J. Climate,* **21,** 2634–2650, doi:10.1175/2007JCLI2012.1.

Chen, M., W. Shi, P. Xie, V. B. S. Silva, V. E. Kousky, R. W. Higgins, and J. E. Janowiak, 2008: Assessing objective techniques for gauge-based analyses of global daily precipitation. *J. Geophys. Res.,* **113,** D04110, doi:10.1029/2007JD009132.

Chou, S.-H., R. Atlas, C.-L. Shie, and J. Ardizzone, 1995: Estimates of surface humidity and latent heat fluxes over oceans from SSM/I data. *Mon. Wea. Rev.,* **123,** 2405–2425, doi:10.1175/1520-0493(1995)123<2405:EOSHAL>2.0.CO;2.

——, E. Nelkin, J. Ardizzone, R. Atlas, and C. L. Shie, 2001: The Goddard satellite-based surface turbulent fluxes dataset version 2 (GSSTF 2.0) [global (grid of 1° × 1°) daily air–sea surface fluxes from July 1987 to December 2000] distributed by Goddard DISC. [Available online at http://disc.sci.gsfc.nasa.gov/gesNews/gsstf_version_3_released.]

——, ——, ——, R. M. Atlas, and C.-L. Shie, 2003: Surface turbulent heat and momentum fluxes over global oceans based on the Goddard satellite retrieval, version 2 (GSSTF2). *J. Climate,* **16,** 3256–3273, doi:10.1175/1520-0442(2003)016<3256:STHAMF>2.0.CO;2.

Clayson, C. A., and A. Bogdanoff, 2013: The effect of diurnal sea surface temperature warming on climatological air–sea fluxes. *J. Climate,* **26,** 2546–2556, doi:10.1175/JCLI-D-12-00062.1.

Compo, G. P., and Coauthors, 2011: The Twentieth Century Reanalysis Project. *Quart. J. Roy. Meteor. Soc.,* **137,** 1–28, doi:10.1002/qj.776.

Dai, A., 2013: The influence of the inter-decadal Pacific oscillation on U.S. precipitation during 1923–2010. *Climate Dyn.,* **41,** 633–646, doi:10.1007/s00382-012-1446-5.

——, I. Y. Fung, and A. D. Del Genio, 1997: Surface observed global land precipitation variations during 1900–88. *J. Climate,* **10,** 2943–2962, doi:10.1175/1520-0442(1997)010<2943:SOGLPV>2.0.CO;2.

Dee, D. P., and Coauthors, 2011: The ERA-Interim reanalysis: Configuration and performance of the data assimilation system. *Quart. J. Roy. Meteor. Soc.,* **137,** 553–597, doi:10.1002/qj.828.

Deser, C., A. S. Phillips, and J. W. Hurrell, 2004: Pacific interdecadal climate variability: Linkages between the tropics and the North Pacific during boreal winter since 1900. *J. Climate,* **17,** 3109–3124, doi:10.1175/1520-0442(2004)017<3109:PICVLB>2.0.CO;2.

Dirmeyer, P. A., X. Gao, M. Zhao, Z. Guo, T. Oki, and N. Hanasaki, 2006: GSWP-2: Multimodel analysis and implications for our

perception of the land surface. *Bull. Amer. Meteor. Soc.,* **87,** 1831–1397, doi:10.1175/BAMS-87-10-1381.

Fairall, C. W., E. F. Bradley, J. E. Hare, A. A. Grachev, and J. B. Edson, 2003: Bulk parameterization of air–sea fluxes: Updates and verification for the COARE algorithm. *J. Climate,* **16,** 571–591, doi:10.1175/1520-0442(2003)016<0571:BPOASF>2.0.CO;2.

Gobron, N., B. Pinty, F. Mélin, M. Taberner, M. M. Verstraete, M. Robustelli, and J.-L. Widlowski, 2007: Evaluation of the MERIS/ENVISAT FAPAR product. *Adv. Space Res.,* **39,** 105–115, doi:10.1016/j.asr.2006.02.048.

Gu, G., R. F. Adler, G. J. Huffman, and S. Curtis, 2007: Tropical rainfall variability on interannual-to-interdecadal and longer time scales derived from the GPCP monthly product. *J. Climate,* **20,** 4033–4046, doi:10.1175/JCLI4227.1.

——, and ——, 2013: Interdecadal variability/long-term changes in global precipitation patterns during the past three decades: Global warming and/or Pacific decadal variability? *Climate Dyn.,* **40,** 3009–3022, doi:10.1007/s00382-012-1443-8.

Hilburn, K. A., and F. J. Wentz, 2008: Intercalibrated passive microwave rain products from the unified microwave ocean retrieval algorithm (UMORA). *J. App. Meteor. Climatol.,* **47,** 778–794, doi:10.1175/2007JAMC1635.1.

——, and C.-L. Shie, 2011: Decadal trends and variability in Special Sensor Microwave/Imager (SSM/I) brightness temperatures and Earth incidence angle. RSS Tech. Rep. 092811, 53 pp. [Available online at http://images.remss.com/papers/tech_reports/hilburn_SSMI_EIA_TB_RSS_Tech_Rpt_092811.pdf.]

Huffman, G. J., R. F. Adler, D. T. Bolvin, and G. Gu, 2009: Improving the global precipitation record: GPCP version 2.1. *Geophys. Res. Lett.,* **36,** L17808, doi:10.1029/2009GL040000.

Jackson, D. L., G. A. Wick, and F. R. Robertson, 2009: Improved multi-sensor approach to satellite-retrieved near-surface specific humidity observations. *J. Geophys. Res.,* **114,** D16303, doi:10.1029/2008JD011341.

Janowiak, J. E., and P. Xie, 1999: CAMS_OPI: A global satellite-rain gauge merged product for real-time precipitation monitoring applications. *J. Climate,* **12,** 3335–3342, doi:10.1175/1520-0442(1999)012<3335:COAGSR>2.0.CO;2.

Jiménez, C., and Coauthors, 2011: Global intercomparison of 12 land surface heat flux estimates. *J. Geophys. Res.,* **116,** D02102, doi:10.1029/2010JD014545.

Josey, S. A., E. C. Kent, and P. K. Taylor, 1998: The Southampton Oceanography Centre (SOC) ocean-atmosphere heat, momentum and freshwater flux atlas. Southampton Oceanography Centre Rep. 6, 30 pp.

Jung, M., M. Reichstein, and A. Bondeau, 2009: Towards global empirical upscaling of FLUXNET eddy covariance observations: Validation of a model tree ensemble approach using a biosphere model. *Biogeosci. Discuss.,* **6,** 5271–5304, doi:10.5194/bgd-6-5271-2009.

——, and Coauthors, 2010: Recent decline in the global land evapotranspiration trend due to limited moisture supply. *Nature,* **467,** 951–954, doi:10.1038/nature09396.

Kanamitsu, M., W. Ebisuzaki, J. Woollen, S.-K. Yang, J. J. Hnilo, M. Fiorino, and G. L. Potter, 2002: NCEP–DOE AMIP-II Reanalysis (R-2). *Bull. Amer. Meteor. Soc.,* **83,** 1631–1643, doi:10.1175/BAMS-83-11-1631.

Kao, H.-Y., and J.-Y. Yu, 2009: Contrasting eastern-Pacific and central-Pacific types of ENSO. *J. Climate,* **22,** 615–632, doi:10.1175/2008JCLI2309.1.

Kummerow, C. D., and Coauthors, 2001: The evolution of the Goddard Profiling Algorithm (GPROF) for rainfall estimation from passive microwave sensors. *J. Appl. Meteor.,* **40,** 1801–1820, doi:10.1175/1520-0450(2001)040<1801:TEOTGP>2.0.CO;2.

——, S. Ringerud, J. Crook, D. Randel, and W. Berg, 2011: An observationally generated a priori database for microwave rainfall retrievals. *J. Atmos. Oceanic Technol.,* **28,** 113–130, doi:10.1175/2010JTECHA1468.1.

Liang, X., E. F. Wood, and D. P. Lettenmaier, 1996: Surface soil moisture parameterization of the VIC-2L model: Evaluation and modification. *Global Planet. Change,* **13,** 195–206, doi:10.1016/0921-8181(95)00046-1.

——, Z. Xie, and M. Huang, 2003: A new parameterization for surface and groundwater interactions and its impact on water budgets with the variable infiltration capacity (VIC) land surface model, *J. Geophys. Res.,* **108,** 8613, doi:10.1029/2002JD003090.

Lee, T., and M. J. McPhaden, 2008: Decadal phase change in large-scale sea level and winds in the Indo-Pacific region at the end of the 20th century. *Geophys. Res. Lett.,* **35,** L01605, doi:10.1029/2007GL032419.

Lorenz, C., and H. Kunstmann, 2012: The hydrological cycle in three state-of-the-art reanalyses: Intercomparison and performance analysis. *J. Hydrometeor.,* **13,** 1397–1420, doi:10.1175/JHM-D-11-088.1.

Lyon, B., and D. G. DeWitt, 2012: A recent and abrupt decline in the East African long rains. *Geophys. Res. Lett.,* **39,** L02702, doi:10.1029/2011GL050337.

——, A. G. Barnston, and D. G. DeWitt, 2013: Tropical Pacific forcing of a 1998–1999 climate shift: Observational analysis and climate model results for the boreal spring season. *Climate Dyn.*, doi:10.1007/s00382-013-1891-9.

McPhaden, M., T. Lee, and D. McClurg, 2011: El Niño and its relationship to changing background conditions in the tropical Pacific. *Geophys. Res. Lett.,* **38,** L15709, doi:10.1029/2011GL048275.

Merrifield, M. A., P. R. Thompson, and M. Lander, 2012: Multidecadal sea level anomalies and trends in the western tropical Pacific. *Geophys. Res. Lett.,* **39,** L13602, doi:10.1029/2012GL052032.

Molod, A., L. Takacs, M. Suarez, J. Bacmeister, I.-S. Song, and A. Eichmann, 2012: The GEOS-5 atmospheric general circulation model: Mean climate and development from MERRA to Fortuna. Tech. Rep. Series on Global Modeling and Data Assimilation NASA/TM–2012-104606, Vol. 28, 124 pp.

Mueller, B., and Coauthors, 2011: Evaluation of global observations-based evapotranspiration datasets and IPCC AR4 simulations. *Geophys. Res. Lett.,* **38,** L06402, doi:10.1029/2010GL046230.

——, and Coauthors, 2013: Benchmark products for land evapotranspiration: LandFlux-EVAL multi-dataset synthesis. *Hydrol. Earth Syst. Sci. Discuss.,* **10,** 769–805, doi:10.5194/hessd-10-769-2013.

Peixoto, J. P., and A. H. Oort, 1992: *Physics of Climate.* American Institute of Physics, 520 pp.

Qian, T., A. Dai, K. E. Trenberth, and K. W. Oleson, 2006: Simulation of global land surface conditions from 1948–2004. Part I: Forcing data and evaluation. *J. Hydrometeor.,* **7,** 953–975, doi:10.1175/JHM540.1.

Reichle, R. H., R. D. Koster, G. J. M. De Lannoy, B. A. Forman, Q. Liu, S. P. P. Mahanama, and A. Toure, 2011: Assessment

and enhancement of MERRA land surface hydrology estimates. *J. Climate,* **24,** 6322–6338, doi:10.1175/JCLI-D-10-05033.1.

——, G. J. M. De Lannoy, B. A. Forman, C. S. Draper, and Q. Liu, 2014: Connecting satellite observations with water cycle variables through land data assimilation: Examples using the NASA GEOS-5 LDAS. *Surv. Geophys.,* **35,** 577–606, doi:10.1007/s10712-013-9220-8.

Reynolds, R. W., T. M. Smith, C. Liu, D. B. Chelton, K. S. Casey, and M. G. Schlax, 2007: Daily high-resolution-blended analyses for sea surface temperature. *J. Climate,* **20,** 5473–5496, doi:10.1175/2007JCLI1824.1.

Rienecker, M. M., and Coauthors, 2011: MERRA: NASA's Modern-Era Retrospective Analysis for Research and Applications. *J. Climate,* **24,** 3624–3648, doi:10.1175/JCLI-D-11-00015.1.

Roberts, J. B., C. A. Clayson, F. R. Robertson, and D. L. Jackson, 2010: Predicting near-surface atmospheric variables from special sensor microwave/imager using neural networks with a first-guess approach. *J. Geophys. Res.,* **115,** D19113, doi:10.1029/2009JD013099.

Robertson, F. R., M. G. Bosilovich, J. Chen, and T. L. Miller, 2011: The effect of satellite observing system changes on MERRA water and energy fluxes. *J. Climate,* **24,** 5197–5217, doi:10.1175/2011JCLI4227.1.

Rodell, M., and Coauthors, 2004: The Global Land Data Assimilation System. *Bull. Amer. Meteor. Soc.,* **85,** 381–394, doi:10.1175/BAMS-85-3-381.

Ropelewski, C. F., and M. S. Halpert, 1987: Global and regional scale precipitation patterns associated with the El Niño/Southern Oscillation. *Mon. Wea. Rev.,* **115,** 1606–1626, doi:10.1175/1520-0493(1987)115<1606:GARSPP>2.0.CO;2.

Rosen, R. D., and A. S. Omolayo, 1981: Exchange of water vapor between land and ocean in the Northern Hemisphere. *J. Geophys. Res.,* **86,** 12 147–12 152, doi:10.1029/JC086iC12p12147.

Saha, S., and Coauthors, 2010: The NCEP Climate Forecast System Reanalysis. *Bull. Amer. Meteor. Soc.,* **91,** 1015–1057, doi:10.1175/2010BAMS3001.1.

Schlosser, C. A., and P. R. Houser, 2007: Assessing a satellite-era perspective of the global water cycle. *J. Climate,* **20,** 1316–1338, doi:10.1175/JCLI4057.1.

Schneider, U., A. Becker, P. Finger, A. Meyer-Christoffer, M. Ziese, and B. Rudolf, 2014: GPCC's new land surface precipitation climatology based on quality-controlled in situ data and its role in quantifying the global water cycle. *Theor. Appl. Climatol.,* **115,** 15–40, doi:10.1007/s00704-013-0860-x.

Sheffield, J., and E. F. Wood, 2007: Characteristics of global and regional drought, 1950–2000: Analysis of soil moisture data from off-line simulation of the terrestrial hydrologic cycle. *J. Geophys. Res.,* **112,** D17115, doi:10.1029/2006JD008288.

——, G. Goteti, and E. F. Wood, 2006: Development of a 50-year high-resolution global dataset of meteorological forcings for land surface modeling. *J. Climate,* **19,** 3088–3111, doi:10.1175/JCLI3790.1.

——, C. R. Ferguson, T. J. Troy, E. F. Wood, and M. F. McCabe, 2009: Closing the terrestrial water budget from satellite remote sensing. *Geophys. Res. Lett.,* **36,** L07403, doi:10.1029/2009GL037338.

Shie, C.-L., and Coauthors, 2009: A Note on reviving the Goddard satellite-based surface turbulent fluxes (GSSTF). Dataset. *Adv. Atmos. Sci.,* **26,** 1071–1080, doi:10.1007/s00376-009-8138-z.

——, K. Hilburn, L. S. Chiu, R. Adler, I.-I. Lin, E. Nelkin, J. Ardizzone, and S. Gao, 2012: Goddard satellite-based surface turbulent fluxes, daily grid *F15*, version 3. Goddard Earth Science Data and Information Services data, doi:10.5067/MEASURES/GSSTF/DATA306.

Syed, T. H., J. S. Famiglietti, D. P. Chambers, J. K. Willis, and K. Hilburn, 2010: Satellite-based global-ocean mass balance estimates of interannual variability and emerging trends in continental freshwater discharge. *Proc. Natl. Acad. Sci. USA,* **107,** 17 916–17 921, doi:10.1073/pnas.1003292107.

Trenberth, K. E., and J. W. Hurrell, 1994: Decadal atmosphere ocean variation in the Pacific. *Climate Dyn.,* **9,** 303–319, doi:10.1007/BF00204745.

——, and C. J. Guillemot, 1998: Evaluation of the atmospheric moisture and hydrological cycle in the NCEP/NCAR reanalyses. *Climate Dyn.,* **14,** 213–231, doi:10.1007/s003820050219.

——, and A. Dai, 2007: Effects of Mount Pinatubo volcanic eruption on the hydrological cycle as an analog of geoengineering. *Geophys. Res. Lett.,* **34,** L15702, doi:10.1029/2007GL030524.

——, L. Smith, T. Qian, A. Dai, and J. Fasullo, 2007: Estimates of the global water budget and its annual cycle using observational and model data. *J. Hydrometeor.,* **8,** 758–769, doi:10.1175/JHM600.1.

——, J. T. Fasullo, and J. Mackaro, 2011: Atmospheric moisture transports from ocean to land and global energy flows in reanalyses. *J. Climate,* **24,** 4907–4924, doi:10.1175/2011JCLI4171.1.

Vermote, E. F., and N. Z. Saleous, 2006: Operational atmospheric correction of MODIS visible to middle infrared land surface data in the case of an infinite Lambertian target. *Science and Instruments,* Vol. 1, J. J. Qu et al., Eds., *Earth Science Satellite Remote Sensing,* Springer and Tsinghua University Press, 123–153, doi:10.1007/978-3-540-37293-6_8.

Wang, W., P. Xie, S.-H. Yoo, Y. Xue, A. Kumar, and X. Wu, 2011: An assessment of the surface climate in the NCEP Climate Forecast System Reanalysis. *Climate Dyn.,* **37,** 1601–1620, doi:10.1007/s00382-010-0935-7.

Wentz, F. J., L. Ricciardulli, K. Hilburn, and C. Mears, 2007: How much more rain will global warming bring? *Science,* **317,** 233–235, doi:10.1126/science.1140746.

——, 2013: SSM/I version-7 calibration report. Remote Sensing Systems Rep. 011012, 46 pp. [Available online at http://images.remss.com/papers/rsstech/.]

Wilheit, T. T., A. T. C. Chang, and L. S. Chiu, 1991: Retrieval of monthly rainfall indices from microwave radiometric measurements using probability distribution functions. *J. Atmos. Oceanic Technol.,* **8,** 118–136, doi:10.1175/1520-0426(1991)008<0118:ROMRIF>2.0.CO;2.

Wisser, D., B. M. Fekete, C. J. Vörösmarty, and A. H. Schumann, 2010: Reconstructing 20th century global hydrography: A contribution to the Global Terrestrial Network-Hydrology (GTN-H). *Hydrol. Earth Syst. Sci.,* **14,** 1–24, doi:10.5194/hess-14-1-2010.

Wong, S., E. J. Fetzer, B. H. Kahn, B. Tian, B. Lambrigtsen, and H.-C. Ye, 2011: Closing the global water vapor budget with AIRS water vapor, MERRA reanalysis, TRMM and GPCP precipitation, and GSSTF evaporation. *J. Climate,* **24,** 6307–6321, doi:10.1175/2011JCLI4154.1.

Yao, Y. J., S. L. Liang, Q. Qin, K. C. Wang, S. M. Liu, and S. H. Zhao, 2012: Satellite detection of increases in global land surface

evapotranspiration during 1984–2007. *Int. J. Digital Earth,* **5,** 299–318, doi:10.1080/17538947.2011.598953, 2012. 773.

Yu, L., 2007: Global variations in oceanic evaporation (1958–2005): The role of the changing wind speed. *J. Climate,* **20,** 5376–5390, doi:10.1175/2007JCLI1714.1.

——, and R. A. Weller, 2007: Objectively analyzed air–sea heat fluxes for the global ice-free oceans (1981–2005). *Bull. Amer. Meteor. Soc.,* **88,** 527–539, doi:10.1175/BAMS-88-4-527.

——, X. Jin, and R. A. Weller, 2008: Multidecade global flux datasets from the Objectively Analyzed Air-Sea Fluxes (OAFlux) Project: Latent and sensible heat fluxes, ocean evaporation, and related surface meteorological variables. Woods Hole Oceanographic Institution, OAFlux Project Tech. Rep. OA-2008-01, 64 pp.

Zhang, Y., J. M. Wallace, and D. S. Battisti, 1997: ENSO-like interdecadal variability: 1900–93. *J. Climate,* **10,** 1004–1020, doi:10.1175/1520-442(1997)010<1004: ELIV>2.0.CO;2.